Supplementary Information for

Operando Identification of Carbon-confined SnO_x Nanodots Dynamics during CO_2-to-formate Electrolysis

Jianing Mao[1,2,3], Bingbao Mei[2*], Shuai Yang[4], Jianrong Zeng[2], Fanfei Sun[2], Wei Chen[3,5], Fei Song[1,2,3*], Zheng Jiang[6*]

Correspondence to: jiangz@ustc.edu.cn; songfei@sinap.ac.cn; meibb@sari.ac.cn

[1] Shanghai Institute of Applied Physics, Chinese Academy of Sciences, Shanghai 201204, PR China.

[2] Shanghai Synchrotron Radiation Facility, Shanghai Advanced Research Institute, Chinese Academy of Sciences, Shanghai 201800, PR China.

[3] University of Chinese Academy of Sciences, Beijing 100049, PR China.

[4] School of Physical Science and Technology, ShanghaiTech University, Shanghai, 201203, PR China.

[5] Low-Carbon Conversion Science and Engineering Center, Shanghai Advanced Research Institute, Chinese Academy of Sciences, Shanghai 201210, PR China.

[6] National Synchrotron Radiation Laboratory, University of Science and Technology of China, Hefei 230026, PR China.

Contents

Methods

Product analysis

Gas products from the outlet of gas chamber were directly transferred into the gas chromatograph (GC-2014, Shimadzu) equipped with a Molecular sieve-13X 60/80 column and a Plot-Q80/100 column during electrochemical reactions and analysed online. H_2 was analysed using a thermal conductivity detector (TCD), and CO or other gaseous hydrocarbons were analysed using a flame ionization detector (FID). A GC run was initiated every 20 min. High purity nitrogen (99.999%) was used as the carrier gas. The Faradaic efficiencies (FEs) of the gas products were calculated by using the concentrations ($C_{product}$) detected by the GC as follows:

$$FE = \frac{C_{product} \times 10^{-6} \times F_{CO_2} \times 10^{-3} \times \alpha \times 96485}{60 \times V_m \times I} \times 100\% \quad (1)$$

where $C_{product}$ (ppm) is the concentration of the gas-phase products, F_{CO2} is the flow rate of CO_2 (10 mL·min^{-1}), α is the quantity of transferred electrons for producing each gas product, V_m (L·mol^{-1}) is the molar volume of gas and I (A) is the electrolysis current.

Liquid products after each constant current electrolysis experiment for 15 min were analyzed and quantified by ^{1}H NMR spectra measured on a 600 MHz NMR spectrometer (Bruker). Before measurement, a 0.5 mL 1 M KOH catholyte solution after CO_2 electrolysis was mixed with 0.1 mL of 5 mM DMSO (HPLC grade, Sigma-Aldrich) in D_2O stock solution. As confirmed by ^{1}H NMR spectra, no liquid products formed after CO_2RR over the used catalysts.

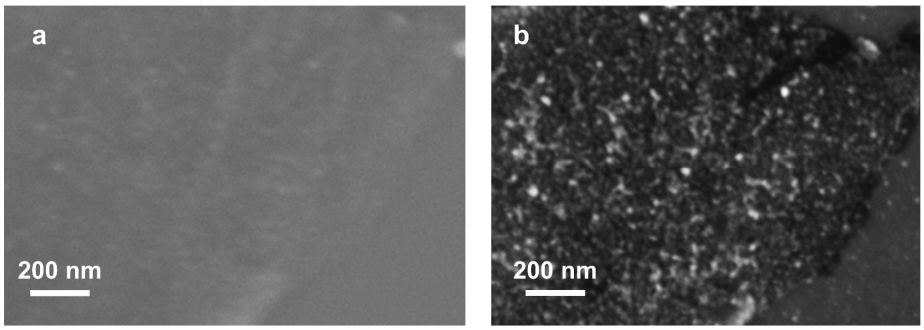

Supplementary Figure 1. SEM images of rGO@SnO_x ND.

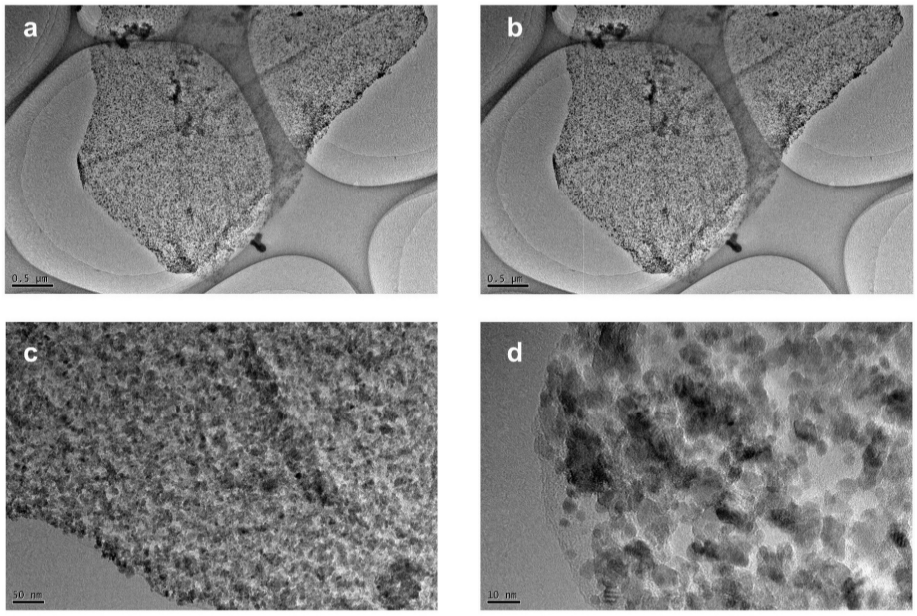

Supplementary Figure 2. TEM images of rGO@SnO_x ND.

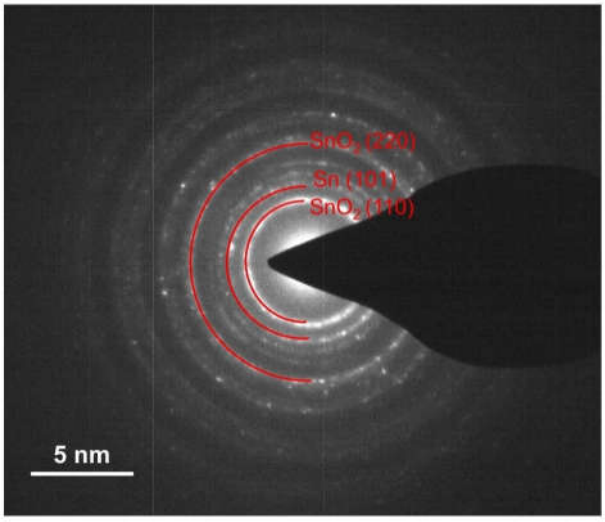

Supplementary Figure 3. SAED pattern of rGO@SnO_x ND.

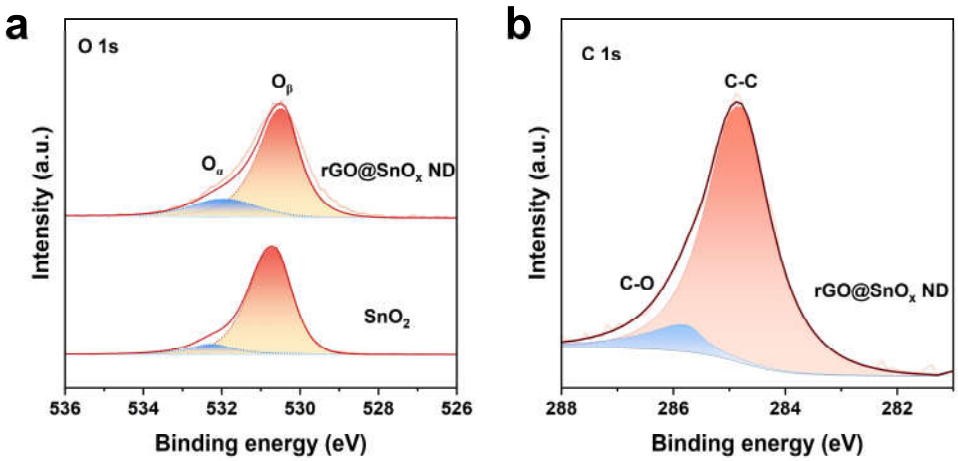

Supplementary Figure 4. (a) O 1s and (b) C 1s XPS spectra of rGO@SnO_x ND and SnO_2.

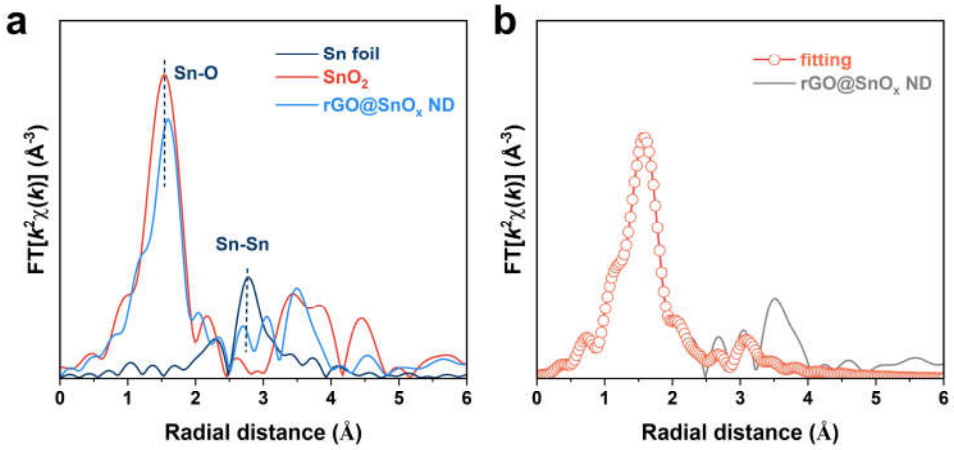

Supplementary Figure 5. (a) Fourier-transformed k^2-weight of Sn K-edge EXAFS spectra of rGO@SnO_x ND, SnO_2 and Sn foil. (b) Fitting of Fourier-transformed k^2-weight of Sn K-edge EXAFS spectra on rGO@SnO_x ND.

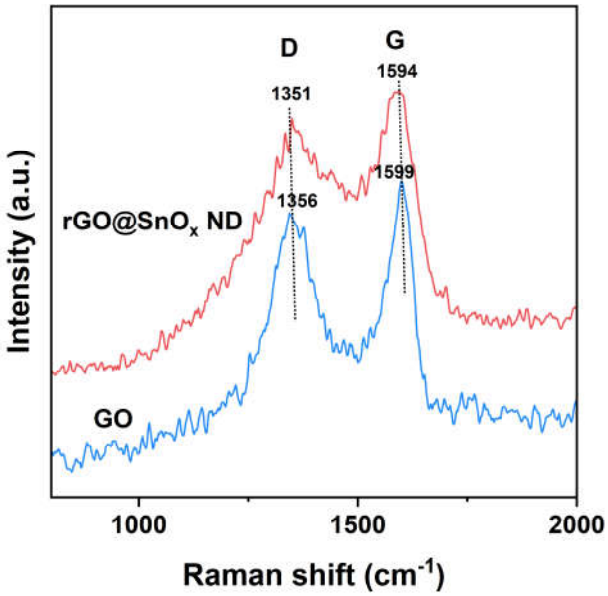

Supplementary Figure 6. Raman spectra of rGO@SnO_x ND and GO.

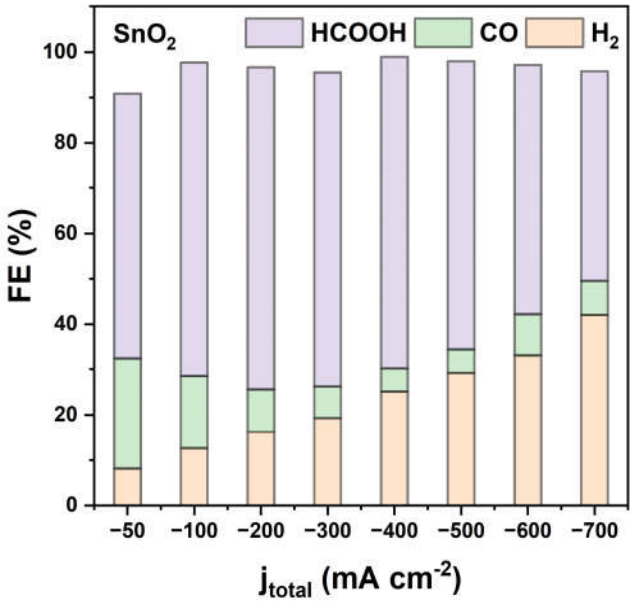

Supplementary Figure 7. Faradaic efficiency of CO_2RR over SnO_2.

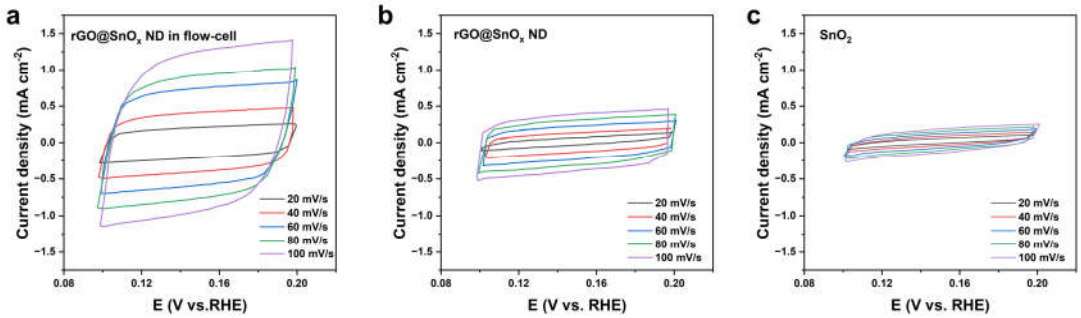

Supplementary Figure 8. Cyclic voltammetry curves of (a) rGO@SnO_x ND in flow cell, (b) rGO@SnO_x ND and (c) SnO_2 in H Cell.

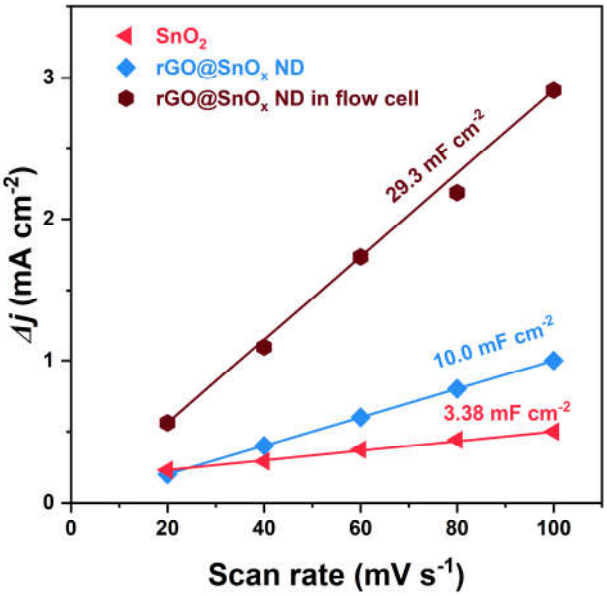

Supplementary Figure 9. The plot of current density against the scan rates.

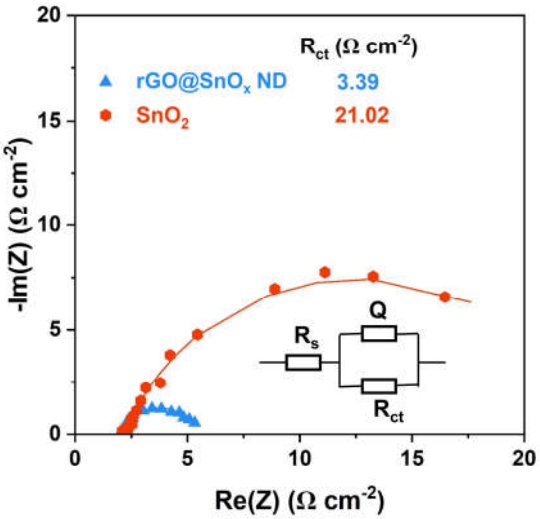

Supplementary Figure 10. EIS test of rGO@SnO_x ND and SnO_2.

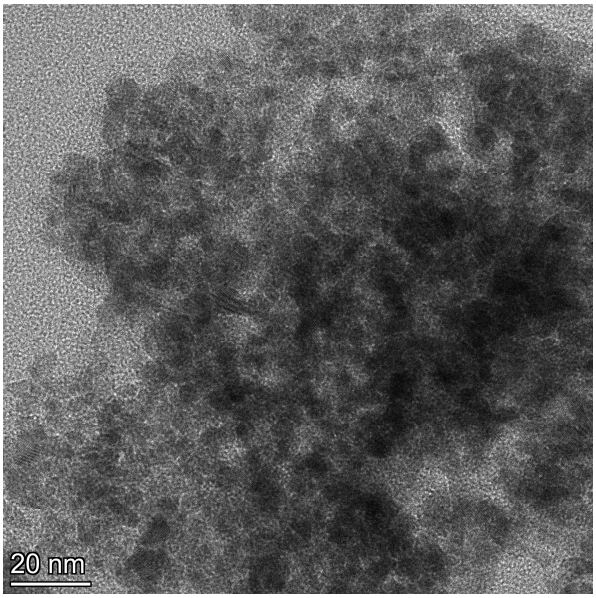

Supplementary Figure 11. TEM image of the rGO@SnO_x ND on carbon paper after reaction.

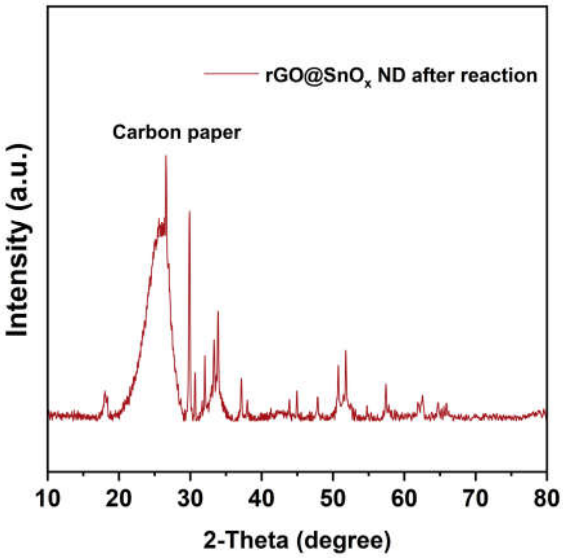

Supplementary Figure 12. Powder XRD pattern of the rGO@SnO_x ND on carbon paper after reaction.

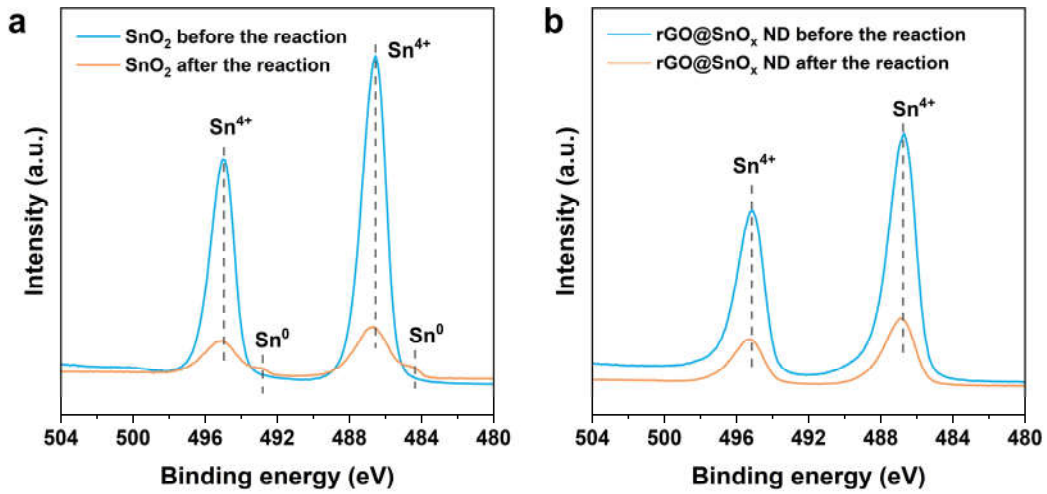

Supplementary Figure 13. NAP-XPS spectra of Sn 3d of (a) SnO_2 and (b) rGO@SnO_x ND before, and after CO_2RR.

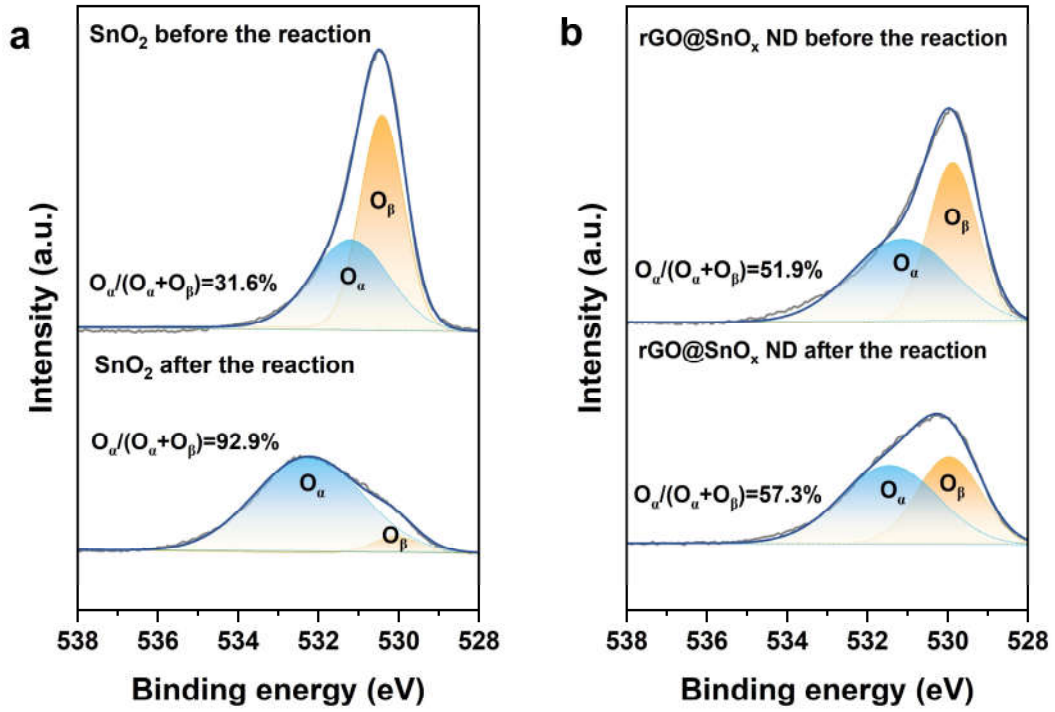

Supplementary Figure 14. NAP-XPS spectra of O 1s of (a) SnO_2 and (b) rGO@SnO_x ND before, and after CO_2RR.

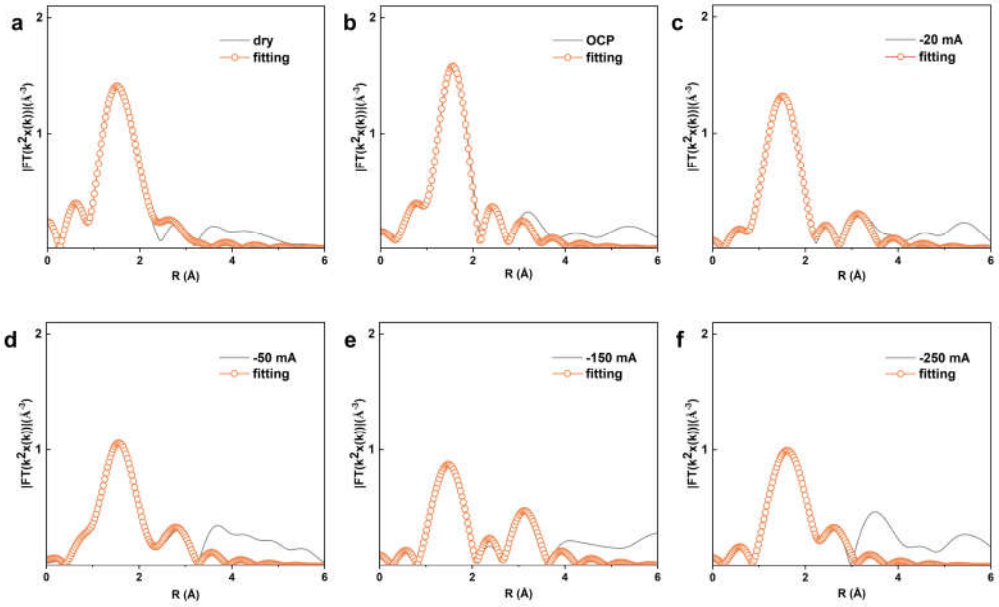

Supplementary Figure 15. (a-f) R-space EXAFS fitting curves of rGO@SnO_x ND under CO_2RR conditions.

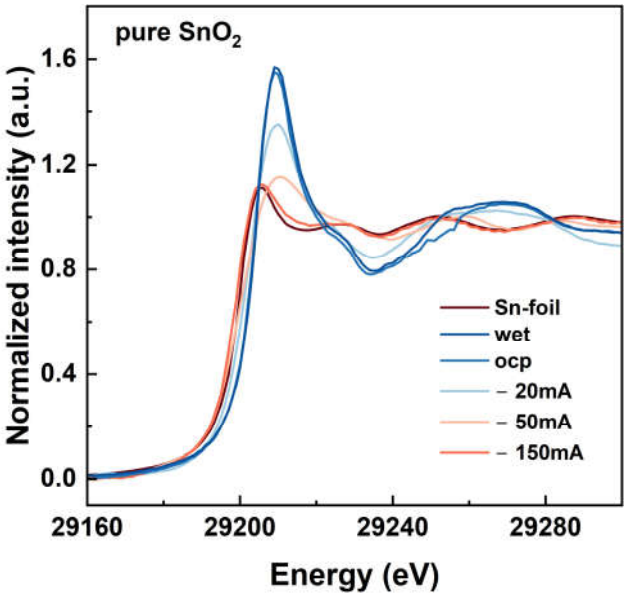

Supplementary Figure 16. Operando Sn K-edge XANES spectra of pure SnO_2.

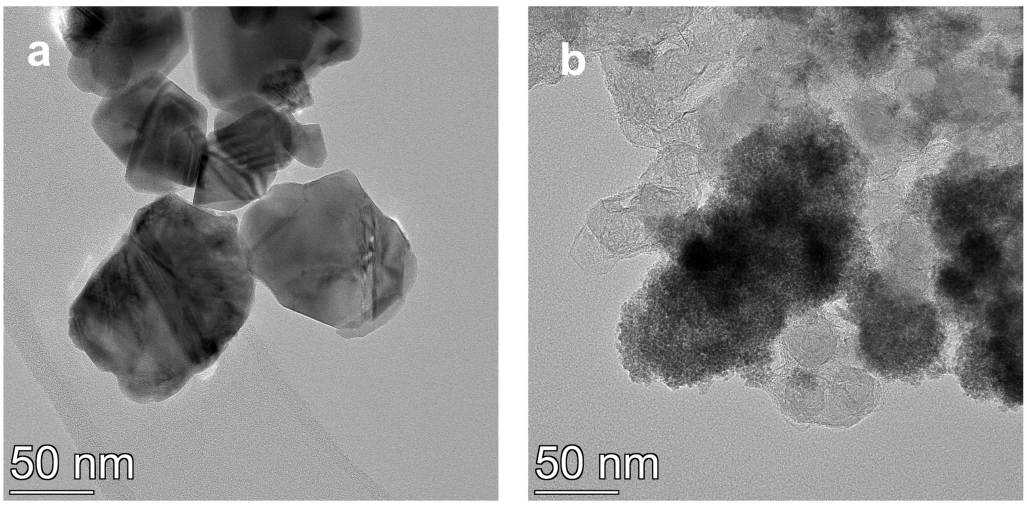

Supplementary Figure 17. a) TEM image of pure SnO_2. b) TEM image of the pure SnO_2 on carbon layer after reaction.

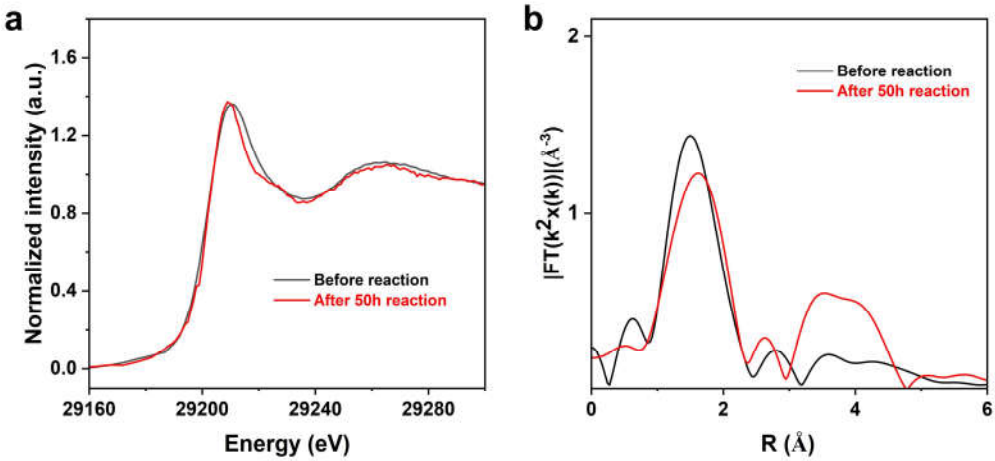

Supplementary Figure 18. (a) XANES and (b) EXAFS of rGO@SnO_x ND before reaction and after the 50 h electrolysis.

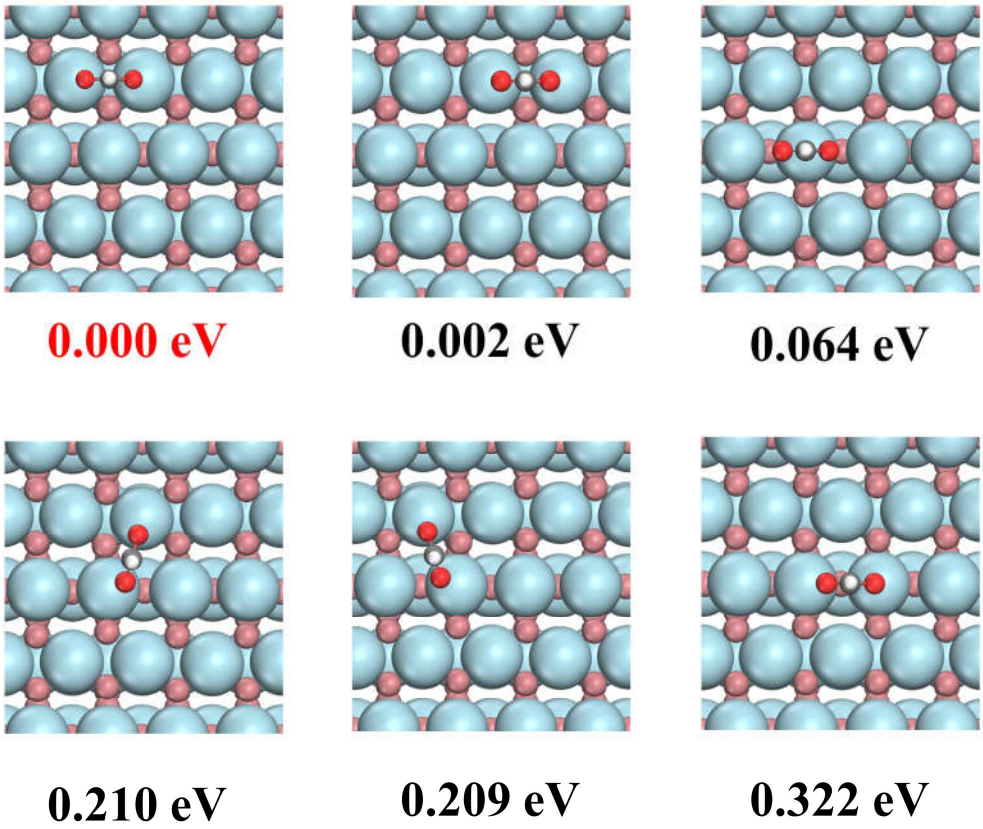

Supplementary Figure 19. Optimized adsorption configurations of HCOO* on the rGO@SnO_x ND ($SRD_{13.3\%}$) and their relative energies.

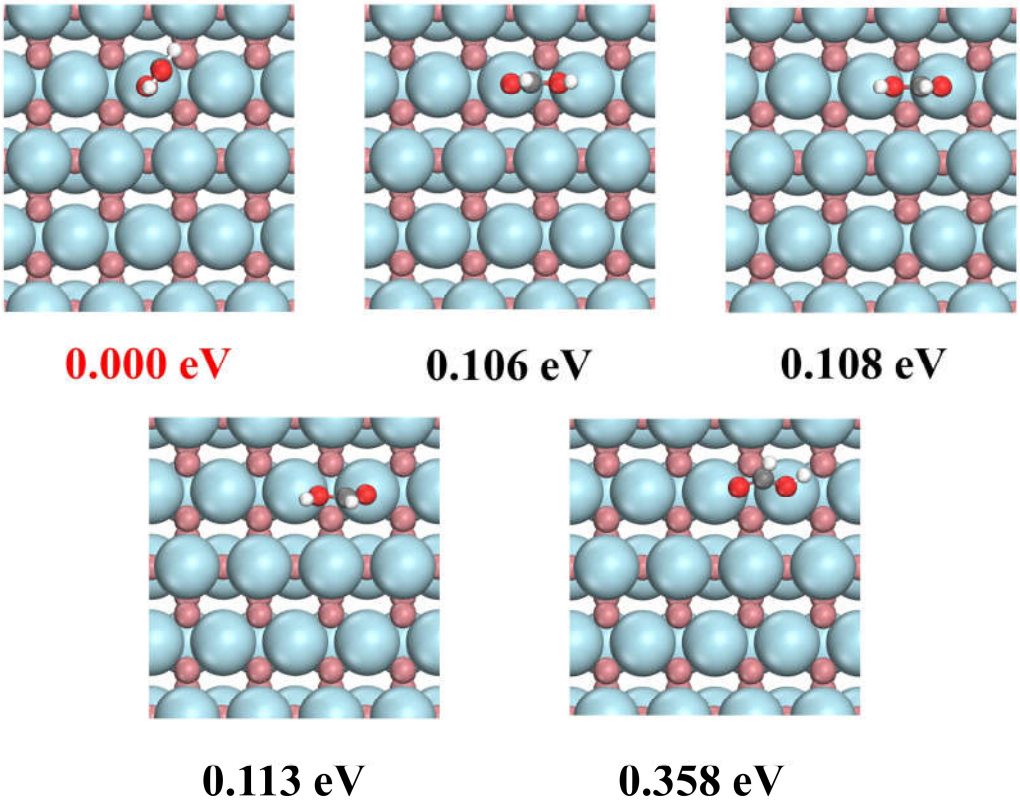

Supplementary Figure 20. Optimized adsorption configurations of *HCOOH on the rGO@SnO_x ND ($SRD_{13.3\%}$) and their relative energies.

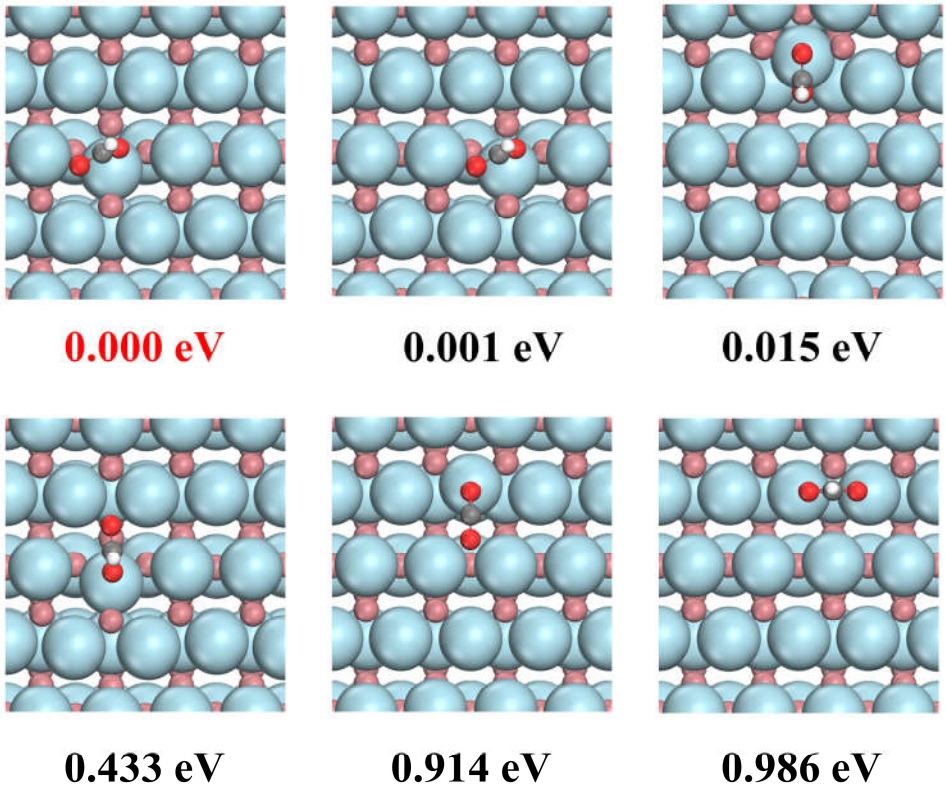

Supplementary Figure 21. Optimized adsorption configurations of HCOO* on the rGO@SnO_x ND ($SRD_{23.8\%}$) and their relative energies.

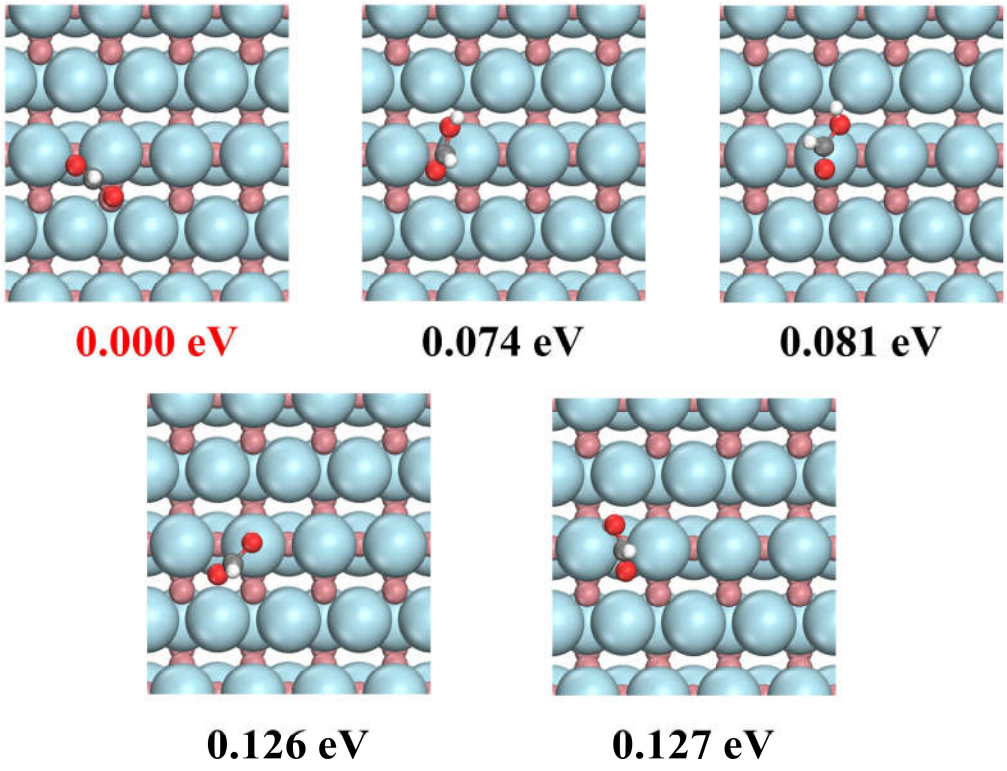

Supplementary Figure 22. Optimized adsorption configurations of *HCOOH on the rGO@SnO_x ND ($SRD_{23.8\%}$) and their relative energies.

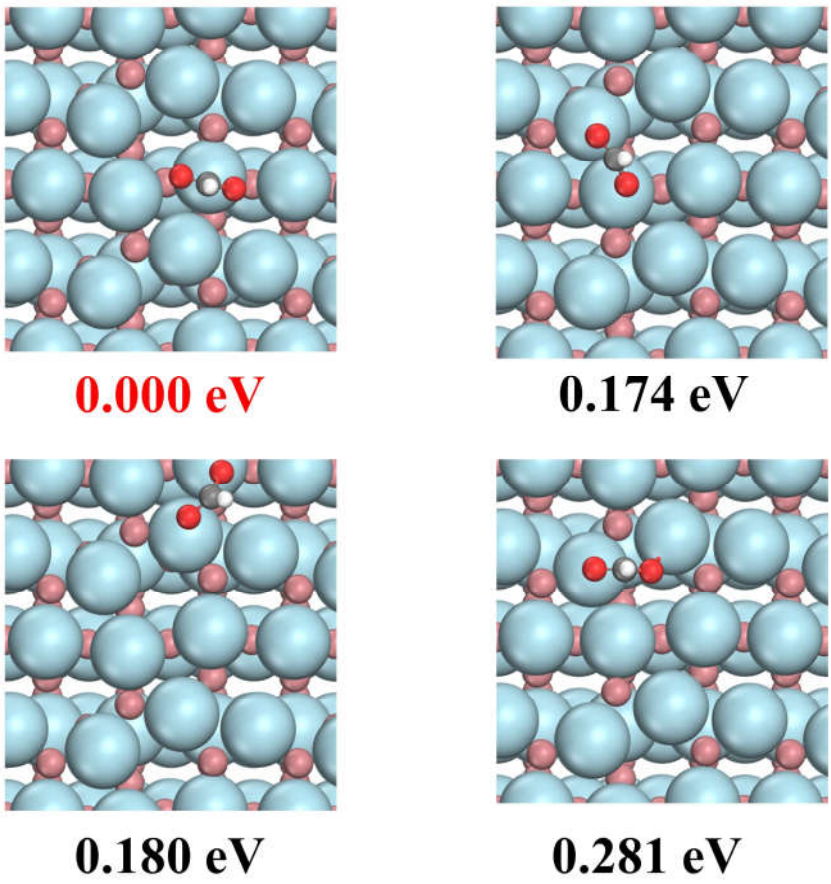

Supplementary Figure 23. Optimized adsorption configurations of HCOO* on the rGO@SnO_x ND ($SRD_{32.3\%}$) and their relative energies.

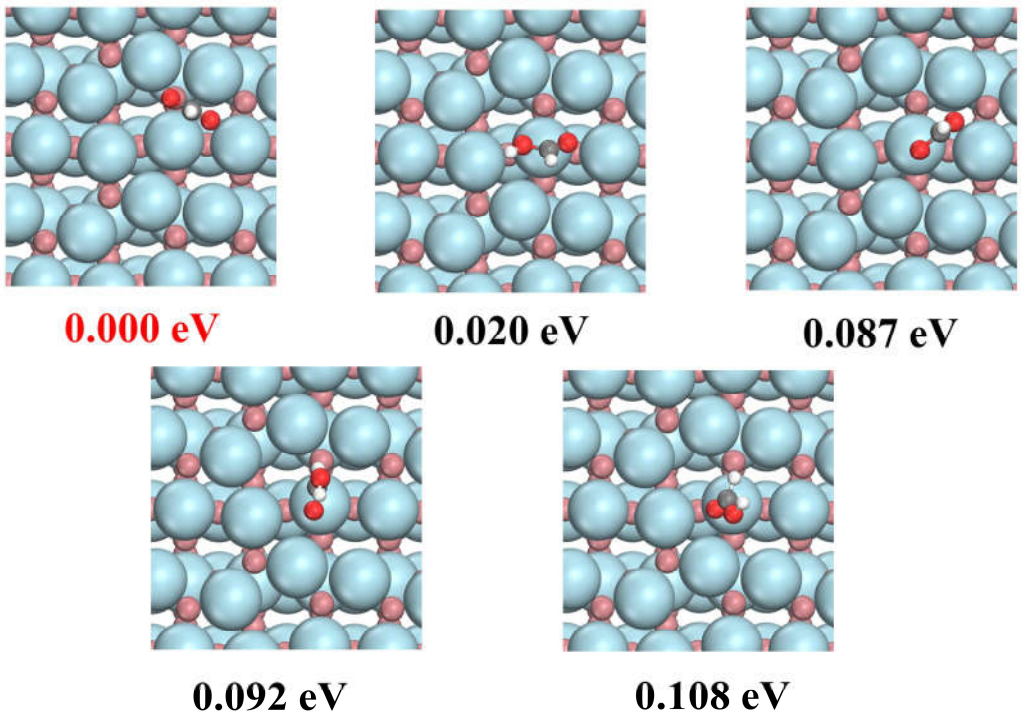

Supplementary Figure 24. Optimized adsorption configurations of *HCOOH on the rGO@SnO_x ND ($SRD_{32.3\%}$) and their relative energies.

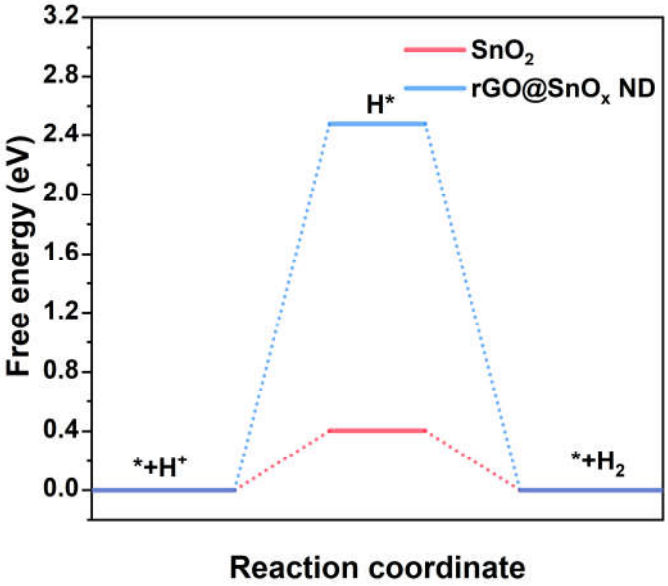

Supplementary Figure 25. Gibbs free energies of the H_2 formation on rGO@SnO_2 ND and SnO_2.

Supplementary Table 1 | Sn K-edge EXAFS curves fitting parameters of rGO@SnOx ND.

Sample	Path	N	R(Å)	σ^2 (10^{-3} Å^2)	ΔE_0 (eV)	R-factor
rGO@SnO$_x$ ND	Sn-O	5.6	2.05	6.0	8.8	0.013
	Sn-Sn	2.0	3.21	10.0	8.8	

Notes: N, coordination number; R, distance between absorber and backscatter atoms; σ^2, Debye-Waller factor; ΔE_0, the edge-energy shift. The S_0^2 values was determined as 0.95.

Supplementary Table 2 | Comparisons of CO2RR-to-formate performance of Sn-based electrodes in flow cell.

Catalyst	FE of HCOOH (%)	|j| of HCOOH (mA cm^{-2})	References
rGO@SnO_x ND	91.7	458	This work
	88	525	
Cu-SnO_2	81	405	[1]
FTO/C	82.5	330	[2]
SnO_2-Bi_2O_3/C HNFs	91	200	[3]
CeO_2-SnO_2 heterostructures	87.1	435	[4]
Bi@Sn NPs	92	230	[5]
SnIn-3 alloy nanoparticles	94	236	[6]
SnO_2/$Bi_2O_3CO_3$ heterojunction	90	200	[7]
Sn NCs	90	90	[8]
NRS-SnO	94	330	[9]
H-Sn_3O_4 NS	91.1	417.2	[10]
Sn(S)-H	72.4	724	[11]
SnO/Cu_xO	62.1	1151.7	[12]

Supplementary Table 3 | Sn K-edge EXAFS curves fitting parameters of rGO@SnO_x ND during CO_2RR conditions.

Sample	Path	N	R(Å)	σ^2 (10^{-3} Å^2)	ΔE_0 (eV)	R-factor
Dry	Sn-O	5.6	2.08	3.0	8.0	0.017
	Sn-Sn	2.0	3.19	6.7	8.0	
OCP	Sn-O	5.6	2.02	3.2	10.0	0.004
	Sn-Sn	2.0	3.16	4.3	10.0	
-20 mA	Sn-O	5.5	2.04	4.3	10.2	0.003
	Sn-Sn	2.3	3.16	4.1	10.2	
-50 mA	Sn-O	5.1	2.07	4.8	8.9	0.004
	Sn-Sn	3.9	3.01	5.3	8.9	
-150 mA	Sn-O	4.7	2.02	9.8	8.9	0.003
	Sn-Sn	4.2	3.21	10.0	8.9	
-250 mA	Sn-O	4.6	2.09	5.6	8.2	0.003
	Sn-Sn	4.9	3.23	3.0	8.2	

Notes: N, coordination number; R, distance between absorber and backscatter atoms; σ^2, Debye-Waller factor; ΔE_0, the edge-energy shift. The S_0^2 values was determined as 0.95.

Supplementary Table 4 | Surface reduction degree of rGO@SnO_x ND during CO_2RR conditions.

Reaction process	Number of O desorption	Surface reduction degree (Number of O desorption / The total number of O)
OCP	0	13.3%
-20 mA	20	16.7%
-50 mA	62	23.8%
-150 mA	102	30.6%
-250 mA	112	32.3%

References

1. Jiang, Y. et al. Stabilizing Oxidation State of SnO_2 for Highly Selective CO_2 Electroreduction to Formate at Large Current Densities. *ACS Catal.* **13**, 3101–3108 (2023).
2. Ko, Y. J. et al. Exploring dopant effects in stannic oxide nanoparticles for CO_2 electro-reduction to formate. *Nat Commun.* **13**, 2205 (2022).
3. Wang, X. et al. Carbon sustained SnO_2-Bi_2O_3 hollow nanofibers as Janus catalyst for high-efficiency CO_2 electroreduction. *Chem. Eng. J.* **426**, 131867 (2021).
4. Liu, H. et al. Ceria -Mediated Dynamic $Sn^0/Sn^{\delta+}$ Redox Cycle for CO_2 Electroreduction. *ACS Catal.* **13**, 5033–5042 (2023).
5. Xing, Y. et al. Bi@Sn Core-Shell Structure with Compressive Strain Boosts the Electroreduction of CO_2 into Formic Acid. *Adv. Sci.* **7**, 1902989 (2020).
6. Wang, J. et al. In-Sn alloy core-shell nanoparticles: In-doped SnO_x shell enables high stability and activity towards selective formate production from electrochemical reduction of CO_2. *Appl. Catal. B* **288**, 119979 (2021).
7. Wang, D. et al. Interfacial engineering of SnO_2/$Bi_2O_2CO_3$ heterojunction on heteroatoms-doped carbon for high-performance CO_2 electroreduction to formate. *Nano Res.* **16**, 2278–2285 (2022).
8. Wang, X. et al. Fu, Y., Atomically dispersed Sn modified with trace sulfur species derived from organosulfide complex for electroreduction of CO_2. *Appl. Catal. B* **304**, 120936 (2022).
9. Qian, Y. et al. Highly efficient electroreduction of CO_2 to formate by nanorod@2D nanosheets SnO, *J. CO_2 Util.* **42**, 101287 (2020).
10. Liu, L. X. et al. Tuning Sn_3O_4 for CO_2 reduction to formate with ultra-high current density. *Nano Energy* **77**, 101287 (2020).
11. Shen, H. et al. Acidic CO_2-to-HCOOH electrolysis with industrial-level current on phase engineered tin sulfide. *Nat Commun* **14,** 2843 (2023).
12. Liu, T. et al. A Tin Oxide-Coated Copper Foam Hybridized with a Gas Diffusion Electrode for Efficient CO_2 Reduction to Formate with a Current Density Exceeding 1 A cm^{-2}. *Small* **18**, e2205323 (2022).